An All-Atom Force Field for Metallocenes

José N. Canongia Lopes,*,† P. Cabral do Couto,§ and Manuel E. Minas da Piedade§

Centro de Química Estrutural, Instituto Superior Técnico, 1049-001 Lisboa, Portugal, and Departamento de Química e Bioquímica, Faculdade de Ciências, Universidade de Lisboa, 1649-016 Lisboa, Portugal

Received: May 11, 2006; In Final Form: October 20, 2006

A new all-atom force field, for the molecular modeling of metallocenes was constructed. Quantum chemical calculations were performed to obtain several force field terms not yet defined in the literature. The remainder were transferred from the OPLS-AA/AMBER framework. The parametrization work included the obtention of geometrical parameters, torsion energy profiles, and distributions of atomic charges that blend smoothly with the OPLS-AA specification for a variety of organic molecular fragments. Validation was carried out by comparing simulated and experimental data for five different ferrocene derivatives in the crystalline phase. The present model can be regarded as a step toward a general force field for metallocenes, built in a systematic way, easily integrated with OPLS-AA, and transferable between different metal−ligand combinations.

Introduction

The molecular models currently used in the area of statistical mechanics—Monte Carlo (MC) and molecular dynamics (MD) simulation methods—are generally developed from force-fields containing both intra- and intermolecular sets of parameters. The latter have a semiempirical nature and are fitted to condensed-phase structural or thermodynamic data; the former can be estimated from quantum mechanical calculations or gas-phase spectroscopic data.

Databases containing force field parameters for a vast selection of inorganic and organic molecules are now available, for instance the OPLS-AA[1] and AMBER[2] force fields. These databases include not only the semiempirical parameters defining the intermolecular interactions between atoms or interacting centers—generally divided into repulsion, dispersion, and electrostatic forces—but also the parameters controlling the geometry and energy of each individual molecule. A significant portion of the existing databases is devoted to organic molecules that are subunits of larger molecules of biological interest, for instance amino acids, sugars or DNA bases. On the other hand, the parametrization of metals or organometallic compounds is comparatively less developed, especially in terms of a force field comprising both inter- and intramolecular interactions. In fact, the area of organometallic molecular modeling exhibits a particularly pronounced difference between the large number and scope of quantum chemical or molecular mechanics studies and their statistical mechanics counterpart.[3−5]

In this paper we report the development of a simple but transferable molecular force-field for MD simulations of metallocenes, to be used within the framework of statistical mechanics. Metallocenes MCp_2 (M = transition metal, Cp = C_5H_5) exhibit a sandwich-like structure with the metal coordinated between two cyclopentadienyl fragments (Figure 1) and constitute a family of molecules whose most well-known member is ferrocene ($FeCp_2$). They are excellent models for systematic studies on how the nature of the metal and the ligand determines the interactions that govern the intermolecular potential since a variety of combinations of metals and substituted Cp rings are possible.[6−8]

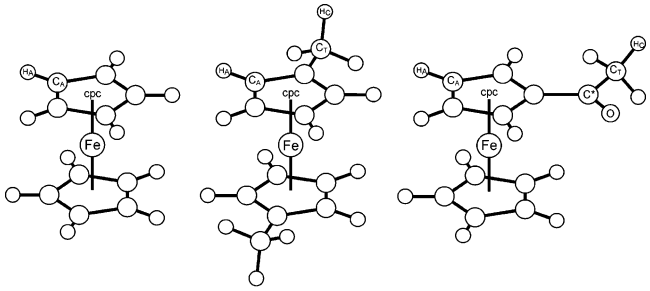

Figure 1. Labeling scheme of ferrocene and of the ferrocene derivatives parametrized in this work. The labeling was based on that used in the AMBER forcefield.[2] The centroid of the cyclopentadienyl ring is denoted by cpc.

Transferability means that the force-field was built in an additive way, starting with the parametrization of a simple force-field for ferrocene, extending it to account for substitution on the Cp rings in other molecules of the ferrocene family (dimethylferrocene, decamethylferrocene, acetylferrocene, and diacetylferrocene), and finally merging the parametrization of the organic residues (methyl, acetyl, etc.) with the values given by the widely used OPLS-AA force field (which borrows its internal parametrization from the AMBER force field). This strategy allows the future generalization of the force field to other families of organometallic compounds in a straightforward and consistent way.

Model Development and Testing

The molecular properties of an isolated ferrocene molecule were taken as the starting point for the development of the present force-field. These were obtained through quantum chemistry calculations performed with the Gaussian 98 program.[9] The choice of ferrocene was an obvious one, given the enormous amount of experimental and theoretical data available

† To whom correspondence should be addressed. E-mail:jmlopes@ist.utl.pt

‡ Centro de Química Estrutural, Instituto Superior Técnico.

§ Departamento de Química e Bioquímica, Faculdade de Ciências, Universidade de Lisboa.

10.1021/jp062896l CCC: $33.50
Published on Web 12/07/2006

TABLE 1: Internal Parametrization of Ferrocene[a]

	d(Fe−C_A)/pm	d(Fe−cpc)/pm	d(C_A−C_A)/pm	d(C_A−H_A)/pm	Tilt(H_A)/deg	ΔE/kJ·ol^{-1}
			LANL2DZ			
HF	225.7 (19.3)	190.5 (24.5)	142.3 (−1.7)	106.8 (−3.6)	−1.0 (−4.7)	0.6 (−3.2)
PW91PW91	208.5 (2.0)	167.8 (1.8)	145.3 (1.3)	108.8 (−1.6)	0.3 (−3.4)	4.7 (0.9)
MPW1PW91	209.1 (2.7)	169.5 (3.5)	143.9 (−0.1)	107.9 (−2.5)	0.5 (−3.2)	3.2 (−0.6)
BPW91	209.0 (2.6)	168.4 (2.4)	145.4 (1.4)	108.8 (−1.6)	0.2 (−3.5)	4.4 (0.6)
B3PW91	209.1 (2.7)	169.4 (3.4)	144.2 (0.2)	108.1 (−2.3)	0.4 (−3.3)	3.4 (−0.4)
B3LYP	212.0 (5.6)	172.8 (6.8)	144.3 (0.3)	108.1 (−2.3)	0.3 (−3.4)	3.0 (−0.8)
			SDDall			
HF	223.2 (16.8)	188.1 (22.1)	141.4 (−2.7)	106.7 (−3.7)	−0.9 (−4.6)	−0.1 (−3.9)
PW91PW91	206.0 (−0.4)	165.4 (−0.6)	144.4 (0.4)	108.6 (−1.8)	0.3 (−3.4)	3.8 (0.0)
MPW1PW91	206.1 (−0.3)	166.4 (0.4)	143.0 (−1.0)	107.8 (−2.6)	0.4 (−3.3)	2.6 (−1.2)
BPW91	206.4 (0.0)	165.9 (−0.1)	144.4 (0.4)	108.6 (−1.8)	0.2 (−3.5)	3.6 (−0.2)
B3PW91	206.3 (−0.1)	166.5 (0.5)	143.3 (−0.7)	107.9 (−2.5)	0.4 (−3.3)	2.8 (−1.0)
B3LYP	209.4 (3.0)	170.1 (4.1)	143.4 (−0.6)	107.9 (−2.5)	0.3 (−3.4)	2.1 (−1.7)
			SDD			
HF	223.5 (17.1)	187.9 (21.9)	142.3 (−1.7)	106.8 (−3.6)	−0.5 (−4.2)	0.7 (−2.9)
PW91PW91	207.0 (0.6)	166.1 (0.1)	145.3 (1.3)	108.9 (−1.5)	0.4 (−3.3)	5.8 (2.0)
MPW1PW91	207.3 (0.9)	167.3 (1.3)	143.8 (−0.2)	107.9 (−2.5)	0.7 (−3.0)	4.1 (0.3)
BPW91	207.4 (1.0)	166.5 (0.5)	145.4 (1.4)	108.9 (−1.5)	0.4 (−3.3)	5.4 (1.6)
B3PW91	207.4 (1.0)	167.3 (1.3)	144.1 (0.1)	108.1 (−2.3)	0.6 (−3.1)	3.4 (−0.4)
B3LYP	210.1 (3.7)	170.5 (4.5)	144.3 (0.3)	108.1 (−2.3)	0.4 (−3.3)	3.9 (0.1)
			Electron Diffraction Data[19]			
ferrocene	206.4 ± 0.3	166.0	144.0 ± 0.2	110.4 ± 0.6	3.4	3.8 ± 1.3
			X-ray Diffraction Data[20−24]			
ferrocene	203 ± 3		141 ± 3	103 ± 5	1.0 ± 1.5	
dimethylferrocene	204 ± 1		142 ± 2	96 ± 1	0.3 ± 0.1	
decamethylferrocene	205 ± 1		142 ± 1			
acetylferrocene	205 ± 2		143 ± 2	101 ± 6	6 ± 4	
diacetylferrocene	205 ± 1		142 ± 2	96 ± 3	1 ± 1	
			Selected Force-Field Parameters			
	206	166	144	108	0.0	3.6

[a] Comparison of DFT results obtained for ferrocene with X-ray and electron diffraction data for ferrocene and its derivatives. The last column contains the energy differences, ΔE, between the staggered and eclipsed conformations of ferrocene in kJ mol^{-1}. All distances are in picometers and the H_A tilt angle (deviation from the Cp ring plane toward the iron atom) is in degrees. The values in parentheses represent the differences between the computed bond distances or conformational energies and the corresponding electron diffraction values.

for this particular molecule. In view of transferability, all the approximations subsequently made in the development of the force field avoided ferrocene-specific assumptions.

Quantum chemistry calculations are relevant for the construction of a consistent molecular force-field in three aspects: (i) definition of molecular equilibrium geometries; (ii) parametrization of the internal force-field using conformational energy profiles; (iii) allocation of partial charges on the interaction centers (ESP charges), through a fit to the molecular electrostatic potential. The strategies and approximations used to combine the computed quantum chemical information with the already available OPLS-AA parametrization in the construction of the present force field are described in the next sections.

Equilibrium Geometry. *DFT Calculations.* It is a well-known fact that metal−ligand bond distances are overestimated when quantum chemistry calculations do not take electron correlation into account.[10] For this purpose, density functional theory (DFT) has proven to be a reliable, economical, and practical approach and was therefore used in the present work.[3,11]

In order to choose an adequate level of theory for molecular structure prediction, the geometry of a single ferrocene molecule with the two Cp rings in eclipsed (D_{5h}) and staggered (D_{5d}) conformations was optimized by using PW91, BPW91, and hybrid MPW1PW91, B3PW91, and B3LYP exchange-correlation functionals[12−15] and LANL2DZ or SDD effective core potentials and split valence basis sets.[16−18]

The iron−carbon, d(Fe−C_A), iron−Cp ring centroid, d(Fe−cpc), carbon−carbon, d(C_A−C_A), and carbon−hydrogen d(C_A−H_A) bond distances, and the tilt angle of the ring hydrogens, Tilt(H_A) (see Figure 1 for labeling scheme of the molecule, consistent with the OPLS-AA/AMBER nomenclature) computed by DFT are compared in Table 1 with the corresponding Hartree−Fock theory (HF) predictions and with experimental electron diffraction (ED)[19] and X-ray diffraction (XRD) data.[20−24] Also included in Table 1 (last column) are the energy differences, ΔE, between the staggered (D_{5d}) and eclipsed (D_{5h}) conformations of ferrocene. As expected, important deviations are found only at the HF level of theory, which overestimates the Fe−C_A or the Fe−cpc distances by ca. 10% and underestimates the experimental ΔE obtained by electron diffraction by 3.0−3.8 kJ·mol^{-1}. The results of the DFT methods are rather similar, with the B3LYP functional consistently giving slightly larger differences on the bond distances than the remaining functionals (ca. 1.5%). On average the best geometrical predictions seem to be those obtained by the BPW91/SDDall level of theory (SDD effective core potentials and triple-ζ valence basis sets on all heavy atoms). This theoretical approach was therefore selected to define the set of structural parameters (bond distances and tilt H_A) given at the bottom of Table 1, which were subsequently used to establish the equilibrium geometry of all the molecules studied in this work.

Intramolecular Force-Field. In the parametrization of the intramolecular force-field the Cp rings of ferrocene, dimethylferrocene, decamethylferrocene, acetylferrocene, and diacetylferrocene were taken as regular pentagons with the C−C and C−H bond distances constrained to 144 and 108 pm, respectively (bottom of Table 1). This type of approximation is common in other force-fields used in MD simulations (for

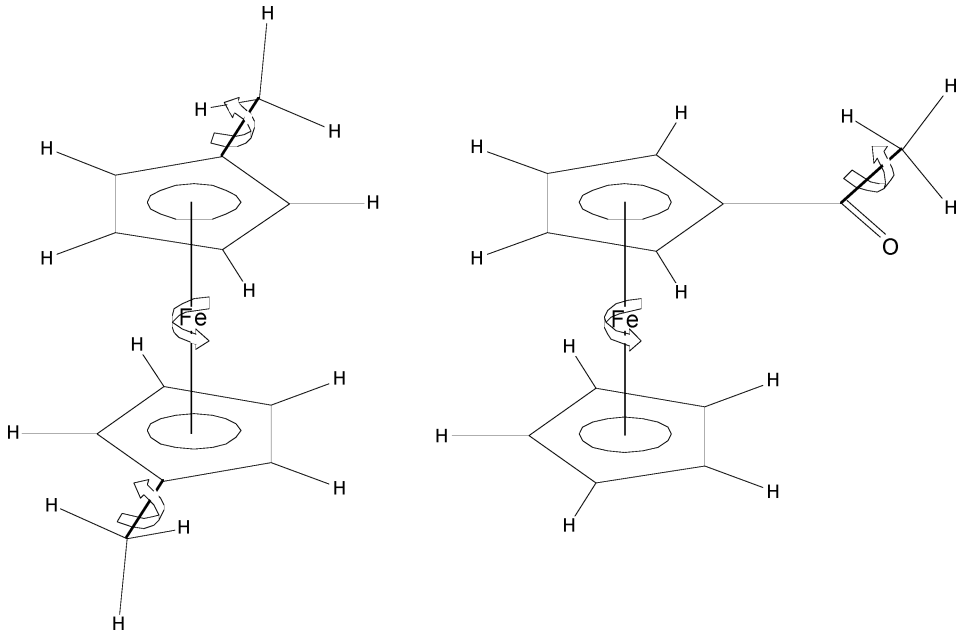

Figure 2. Internal degrees of freedom (internal rotation of the cyclopentadienyl rings and torsion of methyl groups) parametrized in this work.

example, heterocyclic aromatic compounds such as pyrrole, furan, diazole or oxazole are also modeled as rigid units in the OPLS-AA force-field).[25] In the present case it was further supported by the experimental data in Table 1: (i) The size of the ring and its distance from the metal are affected by the environment of the molecule—either isolated or in a crystal lattice. This is apparent in the differences between the corresponding bond lengths obtained by electron diffraction, which refer to the gas phase[19] and by X-ray diffraction, which refer to the crystalline state.[20−24] However, the distortions are such that the ring geometries in five completely different crystals (ferrocene, dimethylferrocene, decamethylferrocene, acetylferrocene, and diacetylferrocene) are comparable and still within the range of the values found for the gaseous ferrocene molecule. (ii) The distortion of the ring caused by different substituent groups is small, which means that the use of a symmetrical ring geometry—a regular pentagon—constitutes a good approximation. The parameters for the bond distances and angles of the methyl and acetyl substituents were directly taken from OPLS-AA.[1]

As a further simplification, the bond distances and angles involving the iron atom and the centroids of the Cp rings were held constant at 206 pm (Table 1), leaving the rotations of the rings around their centroids as the only possible degrees of freedom in the ferrocene molecule—the so-called internal rotations (Figure 2, cf. below). In the case of dimethyl and decamethylferocene the motions associated with the torsion of the methyl groups were also considered. In the acetyl substituents only the torsions of the methyl groups were taken into account, since the carbonyl group is always coplanar with the ring ($C_A-C_A-C^*-O$ dihedral angles of 0 or 180°) due to resonance stabilization.

Internal Rotations. *DFT Calculations.* The torsion potentials corresponding to the dihedral angles between the two Cp rings of ferrocene and dimethylferrocene were obtained from BPW91/SDDall potential energy scans, where a series of values for those dihedral angles were held constant while the remaining internal coordinates of the molecule were allowed to relax to energy minima (Figure 3a).

In the case of ferrocene the torsion potential energy profile obtained at the BPW91/SDDall level of theory was decomposed

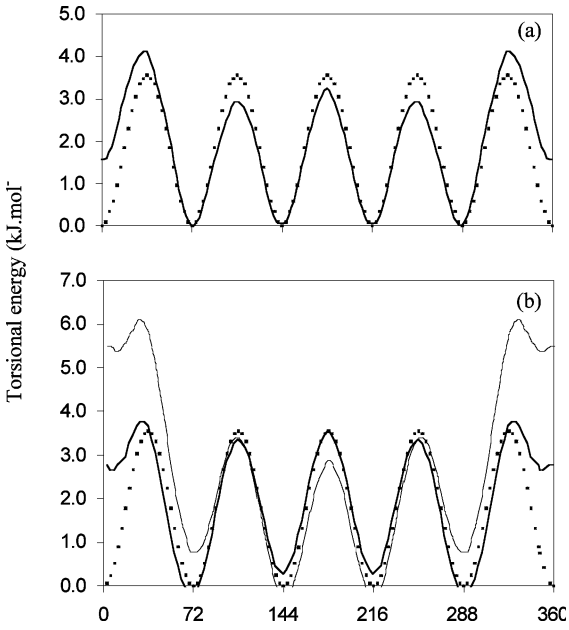

Figure 3. Torsional energy profiles of ferrocene (dotted lines) and dimethylferrocene (solid lines): (a) BPW91/SDDall results. (b) MD results. The thin and thick solid lines refer to a dimethylferrocene forcefield built using the ferrocene dihedral function plus nonbonded contributions with different charge distributions in the Cp rings (see text).

in 25 contributions from the 25 possible (and identical) $C_A-cpc-cpc-C_A$ dihedral angles and described by a simple cosine function of the type $E_{torsion} = A[1 + \cos(B\varphi + C)]$, where φ is the dihedral angle and A, B, and C are the parameters defining the amplitude, frequency and phase of the profile, respectively. The B and C parameters have values of 5 and 180°, respectively, due to the 5-fold symmetry of the Cp rings and the fact that the eclipsed conformations (where all dihedral angles are integer multiples of 72°) correspond to energy minima. The A parameter was fitted to a value of 0.072 kJ·mol^{-1}, corresponding to an energy barrier of 3.6 kJ·mol^{-1}, cf. Figure 3a (dotted line) and Table 1 bottom. In the case of ferrocene the contribution to the torsion potential energy due to nonbonded interactions was found to be negligible: a MD simulation with a single ferrocene

TABLE 2: Point Charges and Van Der Waals Parameters for Ferrocene, Dimethylferrocene, and Acetylferrocene

	Fe	C_A	C_T	C*	H_A	H_C	O
Partial Atomic Point Charges (All in Percent of Atomic Charge Unit)							
DFT (ferrocene)	8.7(±0.7)	−10.0(±0.1)			9.2(±0.1)		
DFT (dimethylferrocene)[a]	9.1(±0.5)	−10(±25)[b]	−25(±2)		10.5(±0.9)	6.9(±0.6)	
DFT (acetylferrocene)[a]	8.2(±0.6)	−9(±5)	−20(±2)	43(±1)	9.9(±0.6)	6(±1)	−46.2(±0.1)
OPLS charges		11.5	−18.0	47.0	11.5	6.0	−47.0
this force-field	**+10**	**−10**	**−18**	**+47**	**+9**	**+6**	**−47**
van der Waals Interactions							
OPLS Parametrization (Lennard-Jones (12−6) Potential)[1]							
ϵ/kJ·mol^{-1}	**2.016**[c]	**0.293**	**0.276**	**0.439**	**0.126**	**0.126**	**0.879**
σ/Å	**3.11**[c]	**3.55**	**3.50**	**3.75**	**2.42**	**2.50**	**2.96**

[a] Geometry computed at the BPW91/SDDall level of theory. [b] Large charge differences due to inductive and hyper-conjugation effects in the Cp ring (see text). [c] Lennard-Jones parameters fitted to the corresponding Buckingham potential curve.

molecule yielded a null torsion energy profile when the only contributions to that energy came from nonbonded interactions (i.e., the *A* parameter is set to zero).

The dimethylferrocene torsion potential energy profile posed a more complex problem. In this case different types of C_A−cpc−cpc−C_A dihedral angles are present (the C_A carbons on the ring can be distinguished by their position relative to the methyl group) and, in addition, the contribution of nonbonding interactions to the torsion energy (steric effects involving the methyl groups and different charge distribution around the Cp rings) is no longer negligible. This means that the presence and nature of the nonbonded interactions must also be taken into account to describe the differences between the torsion potential energy profiles of ferrocene and dimethylferrocene. In fact, in the OPLS-AA force-field, atoms separated by three bonds within the same molecule (a dihedral connection) also interact by Lennard-Jones and electrostatic potentials scaled by a factor of 0.5.

In order to test the importance of the nonbonded interactions in the definition of the torsion potential energy profile of dimethylferrocene several MD simulation runs on single ferrocene and dimethylferrocene molecules were performed. In these runs, the total configuration energy of each molecule was computed for a series of rotation dihedral angles which were kept constant throughout the simulation. The dihedral functions used were those found for ferrocene by the BPW91/SDDall method and the nonbonded interactions were described by the sets of atomic partial charges and van der Waals parameters reported in the following sections. Since other dihedral angles as well as all bond distances and bond angles are constrained in the present model, the profile of the configuration energy as a function of the internal rotation dihedral angle represents the sum of the dihedral function term plus the contribution from the nonbonded interactions. The obtained MD results are shown in Figure 3b, which also includes the BPW91/SDDall profile (dotted line) obtained for ferrocene for comparison purposes. It is clear from Figure 3, parts a and b, that the nonbonded interactions can account for a large part of the differences between the torsion potential energies of ferrocene (dotted line) and dimethylferrocene (thick solid line): deviations between the two profiles are always in the same direction as those found in the DFT calculations. The main departure between the two sets of results is in the energy minimum at 0°, which corresponds to a higher value in the case of the MD calculation since the molecule is not allowed to optimize its geometry by tilting the two Cp rings. It should be noted that, since the two profiles are obtained using different energy minima as reference, their superimposition and comparison provides only a semiquantitative insight on the magnitude of the nonbonded interactions contribution to the overall torsional energy.

If the force-field is slightly modified to account for the different charge distribution among the carbon atoms due to the inductive effect of the methyl group on the cyclopentadienyl ring of dimethylferrocene, then the thin solid line in Figure 3b is obtained. Here the differences are much larger, showing the sensitivity of the torsion potential energy profile to the nature and intensity of the nonbonded interactions.

It must be stressed at this point that the MD calculations on dimethylferrocene were performed keeping the methyl groups in each Cp ring in a fixed orientation that minimizes steric repulsions (holding the H_C−C_T−C_A−Fe dihedral angle at 180°). This is also the lowest energy conformation found in the DFT calculations. If the methyl groups are allowed to rotate and/or other methyl or acetyl groups are added to the molecule, the profiles will suffer further modifications due to the presence of more complex and larger nonbonded contributions. In other words, the deviations from the 5-fold symmetric torsional profile of ferrocene are mainly motivated by nonbonded interactions between ring substituents.

On the basis of the previous conclusion and in order to keep the parametrization of the present force-field as simple and general as possible, the parameters of the internal rotation dihedrals of ferrocene obtained from DFT calculations were used for all ferrocene derivatives and the differences between the corresponding torsion potential energy profiles were assigned exclusively to the existence of diverse and non-negligible nonbonded interactions taken from the OPLS-AA force field (see below).

Partial Charges. Atomic point charges (ESP charges) presented in Table 2 were determined at the BPW91/6-311G-(3df,3pd) level of theory, through a fit to the molecular electrostatic potential, using the CHelpG procedure[15] and the BPW91/SDDall equilibrium geometry. The results for ferrocene correspond to Boltzmann averages of eclipsed and staggered equilibrium conformations (the amplitudes of charge variation due to the differences in conformation are represented by the numbers in parentheses in Table 2). In the case of dimethylferrocene and acetylferrocene the Boltzmann averages of the charges corresponding to minima and maxima of conformational energy (dimethylferrocene: C_T−cpc−cpc−C_T dihedrals of 0, 36, 72, 108, 144, and 180°; acetylferrocene: C_A−cpc−cpc−C_A dihedrals of 0 and 36°), were first computed. The obtained results were then averaged out over all C_A or H_A atoms, yielding the values in Table 2 (in this case the values in parentheses reflect the overall charge variation).

The partial charge distribution in the different ferrocene-like molecules does not exhibit large fluctuations, the only exception being the charge distribution between the aromatic carbons, C_A, in dimethylferrocene. The final parametrization of the atomic point charges (Table 2, values in bold) was established taking

TABLE 3: Density and Crystallographic Properties of Ferrocene Derivatives. Comparison between X-ray Diffraction (XRD) and MD Simulation Data

		ferrocene	dimethylferrocene	decamethylferrocene	acetylferrocene	diacetylferrocene
			Crystallographic Properties			
		ref 20	ref 21	ref 22	ref 23	ref 24
space group		14 ($P2_1/a$)	14 ($P2_1/c$)	64 (*Cmca*)	14 ($P2_1/c$)	14 ($P2_1/c$)
			Simulation Details			
no. molecules		280	240	144	192	216
no. cells		$4 \times 5 \times 7$	$3 \times 5 \times 4$	$3 \times 3 \times 4$	$2 \times 6 \times 2$	$6 \times 3 \times 3$
cutoff distance/Å		16	16	16	16	16
T/K		298	173	298	298	298
			Crystallographic vs Simulated Data			
a/Å	XRD	10.53	12.19	15.21	20.595	5.898
	MD	10.63 ± 0.07	12.18 ± 0.05	15.4 ± 0.1	20.8 ± 0.1	6.02 ± 0.04
b/Å	XRD	7.604	7.466	11.887	5.79	13.036
	MD	7.64 ± 0.02	7.56 ± 0.03	12.2 ± 0.1	5.82 ± 0.03	13.1 ± 0.1
c/Å	XRD	5.921	10.839	9.968	18.84	14.962
	MD	5.94 ± 0.03	$11.04 + 0.04$	9.52 ± 0.06	19.2 ± 0.1	15 ± 0.1
β/deg	XRD	121.05	103.25	90	116.87	90.68
	MD	121.35 ± 0.07	102.6 ± 0.2	87 ± 2	116.7 ± 0.1	91.77 ± 0.06
V/Å^3	XRD	406.166	960.203	1802.227	2004.024	1150.292
	MD	410 ± 1	986 ± 4	1780 ± 9	2061 ± 8	1185 ± 7
ρ/kg·dm^3	XRD	1.521	1.481	1.203	1.512	1.560
	MD	1.506 ± 0.004	1.442 ± 0.006	1.217 ± 0.006	1.470 ± 0.006	1.514 ± 0.009
$\Delta\rho$/%	**MD**	**−0.9**	**−2.6**	**1.2**	**−2.8**	**−2.9**

into account (i) the average values between different conformations of the same molecule and between different ferrocene-like molecules, (ii) rounded values that do not alter the value of the point charge more than 0.05 atomic charge units (acu), and (iii) similarity with the partial charges used in the OPLS-AA force-field for analogous organic residues.

In the case of dimethylferrocene the same C_A values obtained for the other ferrocene molecules and OPLS values for the methyl carbon were selected. This represents a deviation of ca. −0.27 acu in the aromatic carbon directly connected to the methyl group, +0.09 acu in the two aromatic carbons adjacent to it, and +0.07 acu in the aliphatic carbon. To take this fact into account, a new set of charges for each new type of substituted ferrocene would have to be calculated ab initio, which would mean the loss of the transferability and robustness of the model under development. Nevertheless, any future refinements of the present model should address this problem, taking into account polarization effects on the Cp rings or the possibility of conjugation between the ring and its adjacent groups.

Intermolecular Repulsion and Dispersion Forces. The repulsion and dispersion terms of the intermolecular potential were modeled via a Lennard-Jones (12−6) potential with the ϵ and σ parameters taken from the OPLS-AA force-field. When dealing with crystalline structures, the Buckingham potential is usually preferred to the Lennard-Jones potential (as implemented in the OPLS-AA force-field), due to a better description of repulsive forces using an exponential term. The Lennard-Jones (12) term is generally considered too "soft" to correctly describe the repulsion forces in tightly packed structures.[4] On the other hand the OPLS-AA force-field is more complete as regards the parametrization of the van der Waals interactions involving the organic residues present in the metallocene molecules (the Lennard-Jones parameters in this force field were obtained by fitting to condensed-phase thermodynamic properties of a wide variety of organic molecules). The main objective of using the LJ potential in the present simulations was to check if a liquid-oriented force-field (OPLS stands for optimized potentials for liquid simulations) can also be used in the simulation of crystalline phases within the scope of statistical mechanics studies. The values of the Lennard-Jones (12−6) are given in Table 2. The cross interaction parameters (not shown in the table) were calculated using the geometrical mean rule for the parameters ϵ and σ.

Validation

The validation of the proposed force-field was based on simulation results obtained using the molecular dynamics technique, implemented with the DL_POLY software.[26] Since the most common condensed-phase experimental data for metallocenes come from X-ray diffraction studies, the performance of the proposed force-field was tested by estimating the unit cell parameters and density of ferrocene, dimethylferrocene, decamethylferrocene, acetylferrocene, and diacetylferrocene.

The simulation boxes and initial configurations were set taking into account the dimensions and occupancy of the unit cells of each crystalline structure selected from the Cambridge Structural Database (CSD).[20−24] Since the dimensions of the unit cells of these crystals are too small to accommodate a sufficiently large cutoff distance, several cells were stacked together to build a sufficiently large and well proportioned simulation box, with cutoff distances of 16 Å. Long-range corrections were applied beyond the cutoff distance and the Ewald sum method (as implemented by the DLPOLY algorithm[26] with a precision of 10^{-3}) was implemented to take into account the long-range character of the electrostatic interactions. The initial position, orientation, and conformation of each molecule within the simulation box were defined by the lattice coordinates taken from the CSD. Since the overall size of the simulation box is defined by the dimensions of the unit cell of each crystal, simulations with different box sizes and cutoff distances were run to check that the dimensions of the simulation box/cutoff were sufficiently large to make negligible any finite size effects (comparisons from results obtained from simulations with cutoff distances of 10, 14, and 16 Å yielded lattice parameters with precision within a few percent). The simulation details for each crystal are summarized in Table 3 for the larger cutoff distances.

The simulations were performed using a Nosé-Hoover thermostat coupled with an anisotropic Hoover barostat that

allowed the simulation box to change volume and shape under $N-p-T$ conditions. The temperature was fixed to match those used during the crystallographic experiments while the pressure was set to 1 bar. All runs were allowed to equilibrate for a period of 100 ps, followed by production times of 200 ps. These simulation times were found to be appropriate since the initial configurations are close to the equilibrium structure and it is observed that the relaxation is complete before the end of the equilibration period.

It should be noted that the objective of these simulations is not to test the ability of the present force-field to generate the corresponding experimental crystal lattice but simply to check if they are compatible. The stringency of the test was confirmed with simulation runs where ad-hoc parameters were introduced and large distortions of the unit cell parameters of the lattice were observed. For instance, if the spacing between the two Cp rings is increased by 10% the volume increase of the crystal can be as high as 6% and the shifts in the cell parameters even higher and with different signs. The use of an anisotropic barostat coupled with the system allows for a relatively short equilibration period due to the frequent rescaling of the position of the particles. The rather short but effective relaxation time was also confirmed by monitoring the length of the sides and angles of the simulation box as the simulation proceeded through the equilibration period.

Conclusion

The density results are shown in Table 3 and exhibit relative deviations from the corresponding experimental values of the order of a few percent (in most cases underestimating the density by 2−3%). These deviations are of the same order of magnitude as those obtained by other authors when comparing the performance of a given force-field against experimental density data.[1] In our case we used the same simple force-field to calculate the density of five different metallocenes, namely ferrocene, dimethylferrocene, decamethylferrocene, acetylferrocene, and diacetylferrocene. The results are consistent within this family of compounds. The agreement is very good considering that the calculations are purely predictive: all parameters used were either directly taken from the OPLS-AA force-field or obtained from DFT calculations; none was adjusted to match experimental data.

The structural properties of the monoclinic crystals considered in the present study were also correctly predicted by the models. After relaxation, the experimental unit cell dimensions were reproduced with uncertainties of a few tenths of Å in the case of the *a*, *b*, and *c* lengths and up to one degree for the β angle.

While the volumetric behavior of the ferrocene family is correctly captured by the present model, the properties closely related to its energetics (e.g., sublimation enthalpy) will be analyzed in future work. Nevertheless, to confirm the validity of the present model in terms of its energy-dependent parametrization, the standard molar enthalpy of sublimation of ferrocene at 298.15 K was calculated as $\Delta_{sub}H^{\circ}_{m}(FeCp_2) = 76 \pm 3$ kJ·mol^{-1}, from equation:

$$\Delta_{sub}H^{\circ}_{m} = \Delta_{sub}U^{\circ}_{m} + \Delta(PV) = -U^{\circ}_{conf} + RT \qquad (1)$$

where U°_{conf} represents the configurational internal energy of the crystal at 1 bar and 298.15 K. This result is in very good agreement with the value $\Delta_{sub}H^{\circ}_{m}(FeCp_2) = 73.4 \pm 1.1$ kJ·mol^{-1}, at 298.15 K, currently recommended for the use of ferrocene as a standard reference material for enthalpy of sublimation measurements.[27,28]

The obtained results indicate that the present model can be regarded as a step toward a general and simple force-field for metallocenes, built in a coherent way, easily integrated with the OPLS-AA force-field, and transferable within significantly different members of the ferrocene family. The extension of this proposed DFT/MD methodology to metallocenes of other transition metals, in conjunction with accurate enthalpy of sublimation measurements for validation of the energy-dependent parametrization is currently in progress.

Supporting Information Available: Table 1S, parameterization of substituted ferrocenes, and Table 2S, ferrocene FIELD file (input of DLPOLY algorithm). This material is available free of charge via the Internet at http://pubs.acs.org.

References and Notes

(1) (a) Jorgensen, W. L.; Maxwell, D. S.; Tirado-Rives, J. *J. Am. Chem. Soc.* **1996**, *118*, 11225. (b) Kaminski, G.; Jorgensen, W. L. *J. Phys. Chem.* **1996**, *100*, 18010.

(2) Cornell, W. D.; Cieplak, P.; Bayly, C. I.; Gould, I. R.; Merz, K. M.; Ferguson, D. M.; Spellmeyer, D. C.; Fox, T.; Caldwell, J. W.; Kollman, P. A. *J. Am. Chem. Soc.* **1995**, *117*, 5179. Parameters obtained from file parm99.dat corresponding to AMBER versions 1999 and 2002.

(3) Fey, N. *J. Chem. Technol. Biotechnol.* **1999**, *74*, 852.

(4) (a) *Theoretical Aspects and Computer Modelling of the Molecular Solid State*; Gavezzotti, A., Ed.; John Wiley: New York, 1997. (b) *Computational Organometallic Chemistry*; Cundari, T. R., Ed.; Marcel Dekker Inc.: New York, 2003.

(5) Shi, S.; Yan, L.; Yang, Y.; Fisher-Shaulsky, J.; Thacher, T. *J. Comput. Chem.* **2003**, *24*, 1059.

(6) *Cambridge Structural Database*. Allen, F. H.; Kennard, O. *Chem. Design Automation News* **1993**, *8*, 1 and 31−37.

(7) *Metallocenes*; Togni, A., Alterman, R. L., Eds.; Wiley: New York, 1998.

(8) *Comprehensive Organometallic Chemistry III*; Crabtree, R., Mingos, M., Eds.; Elsevier: Amsterdam, 2006; Vol. 4−8.

(9) Frisch, M. J.; Trucks, G. W.; Schlegel, H. B.; Scuseria, G. E.; Robb, M. A.; Cheeseman, J. R.; Zakrzewski, V. G.; Montgomery, J. A., Jr.; Stratmann, R. E.; Burant, J. C.; Dapprich, S.; Millam, J. M.; Daniels, A. D.; Kudin, K. N.; Strain, M. C.; Farkas, O.; Tomasi, J.; Barone, V.; Cossi, M.; Cammi, R.; Mennucci, B.; Pomelli, C.; Adamo, C.; Clifford, S.; Ochterski, J.; Petersson, G. A.; Ayala, P. Y.; Cui, Q.; Morokuma, K.; Salvador, P.; Dannenberg, J. J.; Malick, D. K.; Rabuck, A. D.; Raghavachari, K.; Foresman, J. B.; Cioslowski, J.; Ortiz, J. V.; Baboul, A. G.; Stefanov, B. B.; Liu, G.; Liashenko, A.; Piskorz, P.; Komaromi, I.; Gomperts, R.; Martin, R. L.; Fox, D. J.; Keith, T.; Al-Laham, M. A.; Peng, C. Y.; Nanayakkara, A.; Challacombe, M.; Gill, P. M. W.; Johnson, B.; Chen, W.; Wong, M. W.; Andres, J. L.; Gonzalez, C.; Head-Gordon, M.; Replogle, E. S.; Pople, J. A. *Gaussian 98 (Revision A.10)*; Gaussian, Inc.: Pittsburgh, PA, 2001.

(10) Jensen, F. *Introduction to Computational Chemistry*; John Wiley: Chichester, U.K., 1999; pp 109−112.

(11) Ziegler, T. *Can. J. Chem.* **1995**, *73*, 743.

(12) Perdew, J. P.; Burke, K.; Wang, Y. *Phys. Rev. B* **1996**, *54*, 16533.

(13) Becke, A. D. *Phys. Rev. A* **1988**, *38*, 3098.

(14) Adamo, C.; Barone, V. *J. Chem. Phys.* **1998**, *108*, 664.

(15) Becke, A. D. *J. Chem. Phys.* **1993**, *98*, 5648.

(16) Dunning, T. H., Jr.; Hay, P. J. In *Modern Theoretical Chemistry*; Schaefer, H. F., III, Ed.; Plenum: New York, 1976; Vol. 3; pp 1−28.

(17) (a) Hay, P. J.; Wadt, W. R. *J. Chem. Phys.* **1985**, *82*, 270. (b) Hay, P. J.; Wadt, W. R. *J. Chem. Phys.* **1985**, *82*, 284. (c) Hay, P. J.; Wadt, W. R. *J. Chem. Phys.* **1985**, *82*, 299.

(18) Leininger, T.; Nicklass, A.; Stoll, H.; Dolg, M.; Schwerdtfeger, P. *J. Chem. Phys.* **1996**, *105*, 1052.

(19) Haaland, A.; Nilson, J. E. *Acta Chem. Scan.* **1968**, *23*, 2653.

(20) (a) Takusagawa, F.; Koetzle, T. F. *Acta Crystallogr. Sect. B: Struct. Crystallogr. Cryst. Chem.* **1979**, *35*, 1074. (b) Seiler, P.; Dunitz, J. D. *Acta Crystallogr., Sect. B: Struct. Crystallogr. Cryst. Chem.* **1979**, *35*, 1068. (c) Seiler, P.; Dunitz, J. D. *Acta Crystallogr., Sect. B: Struct. Crystallogr. Cryst. Chem.* **1982**, *38*, 1741. (e) Brock, C. P.; Yigang, Fu. *Acta Crystallogr., Sect. B: Struct. Sci.* **1997**, *52*, 928 (CSD ref codes: FEROCE04−06., 13, 24, 27, 29, 31).

(21) Foucher, D. A.; Honeyman, C. H.; Lough, A. J.; Manners, I.; Nelson, J. M. *Acta Crystallogr., Sect. C: Cryst. Struct. Commun.* **1995**, *51*, 1795 (CSD ref code: ZAYDUY).

(22) Freyberg, D. P.; Robbins, J. L.; Raymond, K. N.; Smart, J. C. *J. Am. Chem. Soc.* **1979**, *101*, 892 (CSD ref code: DMFERR01).
(23) Sato, K.; Konno, M.; Sano, H. *Chem. Lett.* **1982**, 817 (CSD ref code: BIWKEX).
(24) Palenik, G. J. *Inorg. Chem.* **1970**, *9*, 2424 (CSD ref code: DACFER10).
(25) McDonald, N. A.; Jorgensen, W. L. *J. Phys. Chem. B* **1998**, *102*, 8049.
(26) Smith, W.; Forester, T. R. *The DL_POLY Package of Molecular Simulation Routines*; version 2.12, The Council for The Central Laboratory of Research Councils, Daresbury Laboratory, Warrington, U.K., 1999.
(27) Sabbah, R., Ed. Reference Materials for Calorimetry and Differential Thermal Analysis. *Thermochim. Acta* **1999**, *331*, 93.
(28) Chickos, J. S.; Acree, W. E., Jr. *J. Phys. Chem. Ref. Data* **2002**, *31*, 537.